# Crystal Growth of α-HgI 2 by the Temperature Difference Method for High Sensitivity X-ray Detection

**ARTICLE** *in* CRYSTAL GROWTH & DESIGN · MAY 2015

Impact Factor: 4.89 · DOI: 10.1021/acs.cgd.5b00468



**5 AUTHORS**, INCLUDING:

Zhang Zhaojun

Chinese Academy of Sciences

**5** PUBLICATIONS **8** CITATIONS

SEE PROFILE

Wei Zheng

Sun Yat-Sen University

**14** PUBLICATIONS **16** CITATIONS

SEE PROFILE

CRYSTAL GROWTH & DESIGN

Article

pubs.acs.org/crystal

# Crystal Growth of $\alpha$-$HgI_2$ by the Temperature Difference Method for High Sensitivity X-ray Detection

Zhaojun Zhang,[†] Wei Zheng,[‡] Anqi Chen,[‡] Kai Ding,[†] and Feng Huang*[,‡,†]

[†]Key Laboratory of Optoelectronic Materials Chemistry and Physics, Fujian Institute of Research on the Structure of Matter, Chinese Academy of Sciences, Fuzhou, Fujian 350002, China

[‡]State Key Laboratory of Optoelectronic Materials and Technologies, School of Physics and Engineering, Sun Yat-Sen University, Guangzhou, Guangdong 510275, China

**ABSTRACT:** $\alpha$-$HgI_2$ is a promising material for room temperature X-ray detection. A facile temperature difference method is designed to grow $4 \times 4 \times 2$ $mm^3$ $\alpha$-$HgI_2$ bulk crystal from KI aqueous solution. Characterization results indicate the as-grown high quality crystals are single-crystalline and possess a standard bandgap ($E_g$ = 2.16 eV at 300 K) and high electrical resistivity ($10^{10}$ Ω·cm). Utilizing the as-grown crystal, moreover, a photoconductive type prototype X-ray detector is fabricated. The detector behaves at high X-ray sensitivity, which is improved by one order of magnitude in comparison with previous results from solution grown $\alpha$-$HgI_2$. In addition to $\alpha$-$HgI_2$, the crystal growth of other halides materials which are used for X-ray detection, e.g., $PbI_2$, $HgBr_2$, $BiI_3$, may also benefit from the presented temperature difference method.

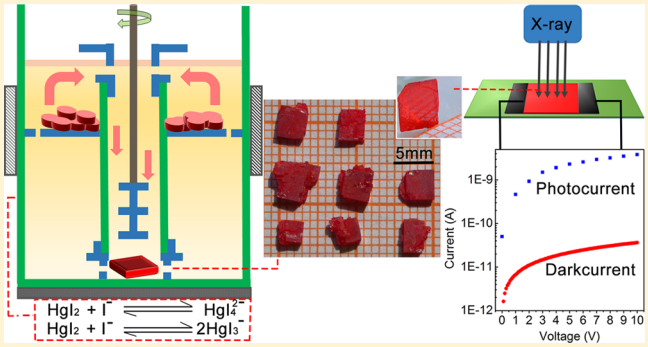


## INTRODUCTION

Room temperature operating semiconductor based X-ray detector plays a typical role in astronomy, biomedical imaging, basic scientific instrumentation, and environmental radioactivity monitoring.[1−4] $\alpha$-$HgI_2$ is the leading candidate material for room temperature X-ray detection due to its bandgap of 2.13 eV, high atom number, and high resistivity of $10^{13}$ Ω·cm.[5−7] For a $\alpha$-$HgI_2$ detector, carriers are generated after $\alpha$-$HgI_2$ absorbing X-ray photon. In addition, the charge collection efficiency, which is directly limited by crystal defects, is an important determinant of the detector performance.[8] Therefore, it is essential to explore crystal growth of high quality $\alpha$-$HgI_2$ crystals.

In general, $\alpha$-$HgI_2$ crystals are grown using solution and vapor growth methods.[9−14] In comparison to vapor phase methods which require high operation temperature, a solution growth method is low-cost and easy-to-operate. Previously reported solution growth methods of $\alpha$-$HgI_2$ bulk crystals generally have employed a solvent evaporation (e.g., ethanol, dimethyl sulfoxide, $CH_3I$, etc.) method.[11,15−18] However, the nonuniform evaporation rate may induce pores and stress defects into the growing $\alpha$-$HgI_2$ crystal,[15] which are unfavorable for the practical use of the crystal.

In addition to the solvent evaporation method, the temperature difference method is also widely used in solution crystal growth but is seldom reported to be applicable for $HgI_2$. Therefore, to overcome the obstacles of the evaporation method, we report herein a temperature difference method with KI aqueous solution as the solvent to grow $\alpha$-$HgI_2$ crystals. The obtained crystal is millimeter-sized, single-crystalline, and possesses low contents of defects and impurities. Additionally, a photoconductive type prototype detector, which is fabricated from the crystal, enables a high sensitivity, fast, and linear response to X-ray. Accordingly, we have demonstrated the practical feasibility of the presented method for growing $\alpha$-$HgI_2$ crystals. Besides, it could also be applied for growing other halides (e.g., $PbI_2$,[19] $HgBr_2$ and $BiI_3$, etc.) which are used for X-ray detection.

## EXPERIMENTAL SECTION

**Crystal Growth.** The crystal growth was performed in a laboratory built apparatus as illustrated in Figure 1. The whole setup was made of a quartz jar which was separated into inner and outer portions by a quartz tube inside it as shown in Figure 1. There were three baffles which were made of Teflon on the two ends and in the middle of the quartz tube, respectively.

The raw material sintered $\alpha$-$HgI_2$ pellets were prepared by heating compressed powder (AR. grade) pellets under nitrogen atmosphere at 120 °C for 2 h. The 0.1 mol/L KI aqueous solution was employed as a solvent. The solution was continuously stirred at a speed of 12 rpm controlled by a stepper motor. Note that a layer of 0.5 mm thick liquid paraffin was spread on the KI solution surface to prevent evaporation. The temperatures of the dissolution zone ($T_1$) and growth zone ($T_2$) were controlled by two heaters independently. First, $T_1$ and $T_2$ were kept the same at 60 °C for 48 h to achieve dissolution equilibrium of $HgI_2$ in the solution. Second, the temperature of dissolution zone ($T_1$)

**Received:** April 4, 2015
**Revised:** May 24, 2015

  

DOI: 10.1021/acs.cgd.5b00468
*Cryst. Growth Des.* XXXX, XXX, XXX−XXX

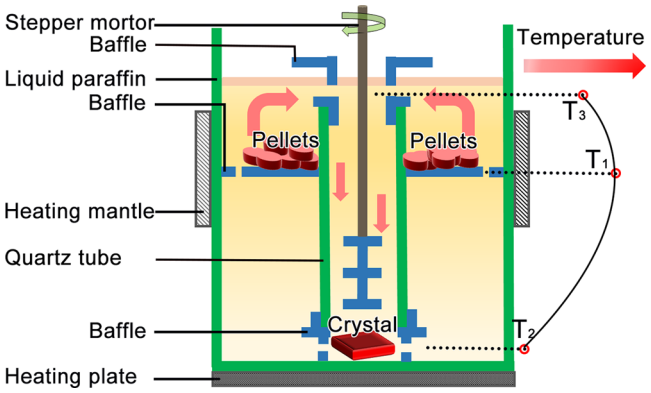


**Figure 1.** Schematic diagram of the cross-section of the crystal growth setup. The used baffles and stirring blades (which are in blue) are all made of Teflon. The stirring rod is made of stainless steel which has good thermal conductivity. The red arrow indicates the direction of flow in the vessel during the crystal growth process.

was increased to 65 °C. As $T_1 > T_3$, the fluid flows into the inside of the vessel relying on the natural Rayleigh−Benard convection. As $T_2 < T_3$, the natural Rayleigh−Benard convection does not occur, while, owing to the forced convection caused by the continuous stirring, the fluid flows to the growth zone at the bottom of the container. Finally, millimeter-sized $\alpha$-$HgI_2$ crystal grains were obtained after about 10 days. The crystal grains were collected, washed with deionized water, and dried for further characterization.

**Single Crystal Characterization.** To identify the crystal structure and phase modification of the crystal, X-ray diffraction ($2\theta$ scans) was performed using a Panalytical X'Pert Pro X-ray diffractometer, using Cu−K$\alpha$ radiation ($\lambda$ = 1.5406 Å). Room temperature Raman scattering spectra ranging from 50 to 300 $cm^{-1}$ were obtained using an excitation 632.8 nm laser by a Jobin Yvon LabRAM HR Raman spectrometer. Energy dispersive X-ray spectroscopy (EDS) was conducted by a Hitachi S-4800 scanning electron microscopy instrument. X-ray photoelectron spectroscopy (XPS) was performed using a Thermo Scientific ESCALAB 250 instrument. Photoluminescence (PL) measurements were performed at 20 K with 325 nm He−Cd laser as the excitation source. The sample used in PL measurement was cut along the {001} plane from bulk $HgI_2$ crystals without further polishing and etching.

**X-ray Detector Measurements.** To determine if the obtained crystal was capable of X-ray detection, the response measurement was performed on the detector fabricated using the naturally cleaved platelet from the as-grown crystal. First, electron beam evaporation was used to deposit Au on $\alpha$-$HgI_2$ crystal surface as contact material. Unfortunately, the crystal surface was damaged heavily after deposition. It is the probably the high electron beam energy that destroyed the crystal. Therefore, like previous practice,[20,21] conductive carbon glue (SPI supplies) was painted on the crystal surface as contact material, and the sample was heated at 60 °C for 30 min to ensure fine contact between carbon layer and the crystal. The dark current of the detector was measured in a shielded chamber using Agilent 4156C precision semiconductor parameter analyzer. X-ray response measurement of the detector was obtained using a Keithley 2602 source/measure unit. X-ray beam was generated by a copper target X-ray tube, whose tube voltage is 30 kVp, and tube current was adjustable from 0 to 5 mA. The distance from X-ray source to detector is 10 cm.

## RESULTS AND DISCUSSION

**Crystal Morphology.** $HgI_2$ is insoluble in water, whereas it is highly soluble in KI aqueous solution owing to the presence of triiodomercurate ($HgI_3^-$) and tetraiodomercurate ($HgI_4^{2-}$) according to the following reversible reactions:[11,17]

$$HgI_2 + 2I^- \rightleftharpoons HgI_4^{2-} \quad (1)$$

$$HgI_2 + HgI_4^{2-} \rightleftharpoons 2HgI_3^- \quad (2)$$

When solution temperature is decreased, chemical equilibrium of eqs 1 and 2 moves to the left. Then $HgI_2$ molecules are dissolved out, and thus crystal growth proceeds. However, the solubility temperature coefficient is extremely small.[17] Therefore, the temperature difference method, which utilized the constant temperature difference to realize sustained growth of crystals, is employed in this system. The obtained crystals are plate-like and around 4 × 4 × 2 $mm^3$ millimeter sized as Figure 2a shows.

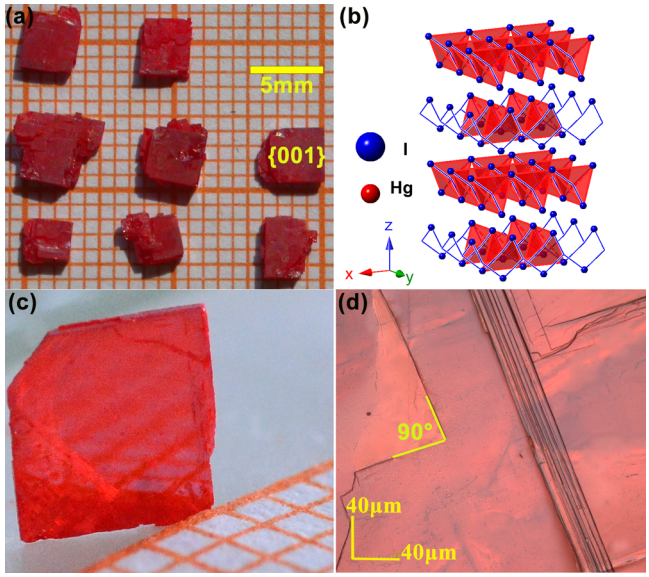


**Figure 2.** (a) The as-grown millimeter-sized $\alpha$-$HgI_2$ crystal. (b) Crystal structure of $\alpha$-$HgI_2$. (c) A naturally cleaved 4 × 4 × 0.5 $mm^3$ platelet which is used for X-ray detector fabrication. (d) The micrograph of freshly cleaved {001} plane of the crystal.

$\alpha$-$HgI_2$ is a layered material which belongs to the space group $P4_2/nmc$, the orderly stacked layers along the $c$-axis are bounded by van der Waals interactions.[22] The four layer structure of $\alpha$-$HgI_2$ crystal is illustrated in Figure 2b. In comparison with the obtained ultrathin layered $PbI_2$ single crystal using the same method,[19] $\alpha$-$HgI_2$ crystal (Figure 2a) appears less layer-like than $PbI_2$. It is possibly because the van der Waals interactions in the $HgI_2$ lattice are stronger than in the $PbI_2$ lattice. Benefiting from the layered characteristic of $\alpha$-$HgI_2$, 4 × 4 × 0.5 $mm^3$ crystal platelet (Figure 2c), which is cleaved along the {001} plane from the crystal, is used for fabricating the X-ray detector. The micrograph of the freshly cleaved {001} plane of the crystal is displayed in Figure 2d. The step edges arranged at a 90° angle are consistent with the crystal symmetry of $\alpha$-$HgI_2$. The oriented cleavage steps on the surface clearly demonstrate the layered structure of $\alpha$-$HgI_2$.[23]

**Structure and Composition Characterization.** As Figure 3a shows, the powder X-ray diffraction (XRD) pattern is in good agreement with standard JCPDS card (No. 01-073-0455) for tetragonal $\alpha$-phase $HgI_2$ with lattice constants of $a = b$ = 4.36 Å, $c$ = 12.45 Å. The XRD pattern of grown bulk crystal only involves (00$l$) diffraction peaks of powder XRD pattern, indicating that the obtained plate-like crystal is oriented in the [001] direction. Room temperature Raman scattering spectrum


DOI: 10.1021/acs.cgd.5b00468
Cryst. Growth Des. XXXX, XXX, XXX−XXX

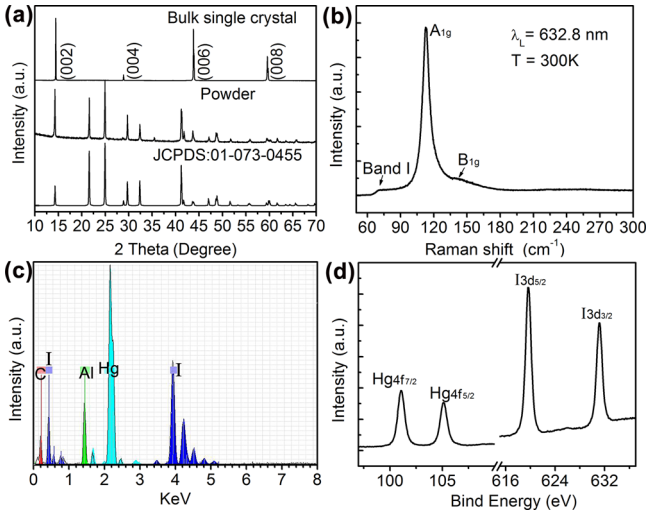


**Figure 3.** (a) X-ray diffraction (XRD) patterns of grown $\alpha$-$HgI_2$ bulk crystal, powder ground from the grown crystal, and standard JCPDS card 01-073-0455, respectively. (b) Room temperature micro-Raman scattering spectrum recorded in back scattering configuration using 632.8 nm laser as excitation. The indicant laser is vertical to the {001} plane of the crystal. (c) EDS spectrum of the crystal. (d) XPS spectrum which shows Hg 4f and I 3d core level.

of the crystal is shown in Figure 3b. For the origin of the weak band I at around 71 $cm^{-1}$, we have check out the phonon dispersion of $\alpha$-$HgI_2$,[24−26] and it is unlikely to be the combination of lower energy mode branch; further studies are required to investigate the origin of this band. $A_{1g}$ vibration mode, which is located at 114 $cm^{-1}$, is the vibration that two I atoms vibrate one against the other while the Hg does not oscillate. And the symmetrical and sharp profile of $A_{1g}$ mode demonstrates the excellent crystallization quality of the crystal. The intensity difference of $A_{1g}$ mode and $B_{1g}$ mode (145 $cm^{-1}$) is the result from the geometry coordination of the Raman scattering measurement.

Figure 3c shows the EDS of as-grown grown $\alpha$-$HgI_2$, confirming that the obtained crystal is pure $HgI_2$. Peaks of Al come from the used sample holder in the EDS test. Peaks of C may come from the absorption of carbon oxides on the sample or the organics in the measurement environment. The liquid paraffin may also introduce C into the sample. It should be mentioned that there is no appearance of K in the crystal in our measurement, indicating the absence of solvent inclusion in our sample. According to a previous report, owing to evaporation of surface evaporation on crystals, the calculated atom ratio of I/Hg from EDS is larger than a stoichiometric sample.[18] And the atom ratio value from our EDS test is 2.164. Note that the one obtained from the XPS test is 2.33. Actually, in the XPS results of the other sample which are measured along with $HgI_2$ in the same batch measurement, although has no Hg contents primarily, peaks of Hg were also observed. Therefore, the surface evaporation of $HgI_2$ in a vacuum could not be ignored. As the measurement period of our EDS test is shorter than XPS, the surface evaporation of the sample in EDS test is smaller. Thus, we believe that the value of 2.164 is closer to the actual value of the sample. Figure 3d plots high-resolution spectra of Hg 4f and I 3d electrons, respectively. The peaks appearing at the binding energy of 101.08 and 105.1 eV are the characteristics for Hg $4f_{7/2}$ and Hg $4f_{5/2}$ core levels. Peaks at about 619.67 and 631.1 eV essentially provide confirmation of I $3d_{5/2}$ and I $3d_{3/2}$.[27] The symmetry Gaussian profile of XPS spectrum pattern indicates that there is no obvious valence deviations of $Hg^{2+}$ and $I^-$; that is, there is no obvious vacancy or interstitial defects in the lattice.

**Optical Properties Characterization.** PL spectrum at 20 K is plotted on a logarithmic scale as Figure 4a shows. And the

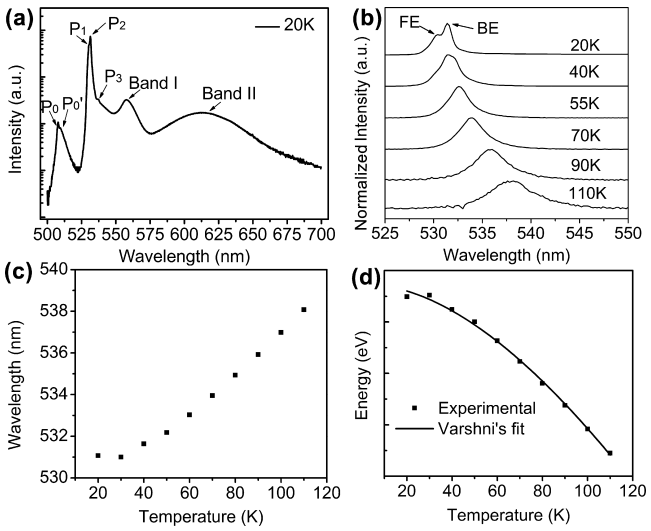


**Figure 4.** (a) 20 K PL spectrum on a logarithmic scale excited by 325 nm laser. (b) The evolution of band-edge emission (normalized) of the sample for varying temperature. At 20 K, the bound exciton (BE) and free exciton (FE) peaks are separated. At 40 K, the BE and FE emission are nearly unresolved. (c) The peak position of band-edge emission are explicitly plotted as a function of temperature by extracting centers from the Lorentzian fits. (d) Evolution of the optical gap in dependence of temperature. The fitting results using Varshni's model is shown as a solid line.

rich fine structure of the spectrum demonstrates the high quality of the crystal structure. The peaks labeled $P_1$ and $P_2$ belong to band-edge luminescence and are originated from free exciton (FE) and bound excitons (BE) emission, respectively.[28,29] Peak $P_3$ is assigned as phonon replicas of $P_1$ and $P_2$.[30,31] The band I centered at 558 nm is related to excitons trapped at mercury vacancies.[30] The weak broad emission band II centered at about 616 nm is generally assigned as radiative recombination of electrons-hole pairs at extrinsic impurity centers.[31,32] The peaks labeled $P_0$ and $P_0'$ centered at around 510 nm may come from yellow modification of $HgI_2$.[33] The laser heating effects on the sample during PL measurement is responsible for the appearance of the yellow modification.

The dependence of band-edge emission (in normalized intensity) on varying temperature is plotted in Figure 4b. The emission position in wavelength shows a clear upward shift as temperature increases. We fit the emission peak with Lorentzian lineshapes, and the peak position is explicitly plotted as a function of temperature by extracting the centers from Lorentzian fits (Figure 4c). Accordingly, the optical bandgap, which was evaluated via its relation to the peak position, displays a clear downshift in energy as temperature increases (Figure 4d). The fitting result (solid line in Figure 4d) demonstrates that the optical gap possesses a typical Varshni-type behavior as $E_g(T) = E_g(0) - (\alpha \times T^2)/(T + \beta)$[35] with $\alpha$ = $1.2 \times 10^{-3}$ eV/K, $\beta$ = 321 K, and $E_g$ (0) = 2.34 eV. And the calculated $E_g$ (300 K) equals 2.16 eV, which agrees with


DOI: 10.1021/acs.cgd.5b00468
Cryst. Growth Des. XXXX, XXX, XXX−XXX

previous report values of 2.13 eV within the uncertainty of the measurements.[36,37]

**X-ray Response Characterization.** Operation dark current of the detector, which decides the dark signal and noise, is a determinant of the detector performance. Considering the high resistivity of the $HgI_2$ crystal, the dark current of the detector was measured in a shielded chamber using a high precision semiconductor parameter analyzer. In addition to dark current, the photo/dark current ratio is another decisive parameter which determines the sensitivity of the detector. And the X-ray response of the detector was measured in home-assembled system as illustrated in Figure 5a.

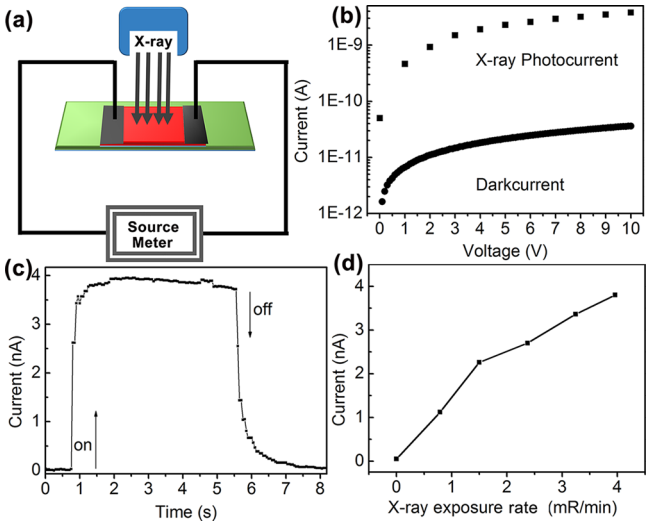


**Figure 5.** (a) Schematic representation of the X-ray response measurement system. (b) The current−voltage curves of the detector illuminated under X-ray exposure of 3.96 mR/min and under dark conditions, respectively. (c) Time-dependent photocurrent of the device with 10 V bias under X-ray exposure of 3.96 mR/min. As the X-ray illumination is turned on, the rise time is only 0.1 s; as the illumination is turned off, the fall time is 0.15 s. (d) Photocurrent of the device with 10 V bias under different X-ray exposure rates.

The dark current and photocurrent of the detector are plotted in Figure 5b. The dark current is about 38 pA at 10 V bias, and using geometrical factors, and the resistivity is estimated to be $10^{10}$ Ω·cm, although this value is two orders of magnitude smaller than that ($10^{13}$ Ω·cm) of vapor grown $\alpha$-$HgI_2$ crystal.[9] The resistivity of $10^{10}$ Ω·cm sufficiently satisfies the requirement of a $\alpha$-$HgI_2$ based X-ray detector.[38] The photocurrent approaches 3.9 nA at 10 V bias under an X-ray exposure of 3.96 mR/min. And the photo/dark current ratio is 102.7, demonstrating the detector's significant response to X-ray. Despite the fact that the X-ray exposure (3.96 mR/min) employed is much less than that in X-ray mammographic energy range used in previous report,[15,18] the photo/dark current ratio of the detector (102.7) is much higher than previous reported values (13.5[15] and 25[18]). The time-dependent photocurrent of the detector with 10 V bias under X-ray exposure of 3.96 mR/min is plotted in Figure 5c. As the time interval in every two data points is 0.05 s, the derived rise time and fall time are 0.10 and 0.15 s, respectively. It should be mentioned that in this study, we used painting carbon glue manually as the electrode owing to the lack of proper electrode deposition techniques, and the electrodes distance on our detector is as large as 1 mm. We believe the photo/dark ratio and response time could be further improved with decreased space gap of the electrodes if an appropriate electrode deposition method were used. In order to evaluate detector linearity at different X-ray exposure rates, the photocurrent of the detector under different X-ray exposure rate was plotted in Figure 5d. It shows that the detector respond nearly linearly to X-ray exposure rate. This makes the detector proper for the quantification of X-ray radiation detection.

## CONCLUSIONS

In conclusion, we have first developed temperature difference method to grow $\alpha$-$HgI_2$ bulk single crystal from KI aqueous solution. Characterization results indicate the as-grown crystals are single-crystalline and possess standard bandgap and high electrical resistivity. Facilitated by the excellent crystal quality, the fabricated photoconductive detector has a low dark current and high sensitivity, fast and linear response to X-ray exposure, which would meet most of the requirements for room temperature X-ray detection. Besides, this approach also provides a meaningful reference for crystal growth of other halides which are used for X-ray detection, such as $PbI_2$, $HgBr_2$, and $BiI_3$.

## AUTHOR INFORMATION

### Corresponding Author

*E-mail: huangfeng@mail.sysu.edu.cn. Phone: +86-020-39943559.

### Notes

The authors declare no competing financial interest.

## ACKNOWLEDGMENTS

This work was financially supported by National Nature Science Foundation of China (NSFC 61474121, 91333207), and Guangdong Natural Science Foundation (2014A030310014). We would like to thank Lu Yang, Yanyan Wu, and Zhaoyun Guan, State Key Laboratory of optoelectronic Materials and Technologies, School of Physics and Engineering, Sun Yat-Sen University, for supporting the optical and electrical properties characterization.

## REFERENCES

(1) Piechotra, M. *Mater. Sci. Eng. R.* **1997**, *18*, 1.
(2) McGregor, D. S.; Hermon, H. *Nucl. Instrum. Methods Phys. Res., Sect. A* **1997**, *395*, 101.
(3) Owens, A.; Peacock, A. *Nucl. Instrum. Methods Phys. Res., Sect. A* **2004**, *531*, 18.
(4) Stoumpos, C. C.; Malliakas, C. D.; Peters, J. A.; Liu, Z.; Sebastian, M.; Im, J.; Chasapis, T. C.; Wibowo, A. C.; Chung, D. Y.; Freeman, A. J.; Wessels, B. W.; Kanatzidis, M. G. *Cryst. Growth Des.* **2013**, *13*, 2722.
(5) Schieber, M.; Roth, M.; Schnepple, W. F. *J. Cryst. Growth* **1983**, *65*, 353.
(6) Jiang, H.; Zhao, Q.; Antonuk, L. E.; El-Mohri, Y.; Gupta, T. *Phys. Med. Biol.* **2013**, *58*, 703.
(7) Park, J. C.; Jeon, P. J.; Kim, J. S.; Im, S. *Adv. Healthcare Mater.* **2015**, *4*, 51.
(8) Zuck, A.; Schieber, M.; Khakhan, O.; Burshtein, Z. *IEEE Trans. Nucl. Sci.* **2003**, *50*, 991.
(9) Swierkowski, S. P.; Armantrout, G.; Wichner, R. *IEEE Trans. Nucl. Sci.* **1974**, *21*, 302.
(10) Schieber, M.; Schnepple, W. F.; Van den Berg, L. *J. Cryst. Growth* **1976**, *33*, 125.
(11) Nicolau, I. F. *J. Cryst. Growth* **1980**, *48*, 51.
(12) Burger, A.; Levi, A.; Nissenbaum, J.; Roth, M.; Schieber, M. *J. Cryst. Growth* **1985**, *72*, 643.


DOI: 10.1021/acs.cgd.5b00468
*Cryst. Growth Des.* XXXX, XXX, XXX−XXX

(13) Piechotka, M. *J. Cryst. Growth* **1995**, *146*, 1.
(14) Douglas, S.; Ariesanti, E. *J. Cryst. Growth* **2013**, *379*, 7−15.
(15) Ugucioni, J. C.; Netto, T. G.; Mulato, M. *Nucl. Instrum. Methods Phys. Res., Sect. A* **2010**, *615*, 259.
(16) Rao, M.; Verma, J.; Patro, A. *J. Phys. D, Appl. Phys.* **1980**, *13*, 1545.
(17) Fornaro, L.; Luchini, L.; Kőncke, M.; Mussio, L.; Quagliata, E.; Chattopadhyay, K.; Burger, A. *J. Cryst. Growth* **2000**, *217*, 263.
(18) Caldeira, A. M. F.; Ugucioni, J. C.; Mulato, M. *Nucl. Instrum. Methods Phys. Res., Sect. A* **2014**, *737*, 87.
(19) Zhang, J.; Song, T.; Zhang, Z.; Ding, K.; Huang, F.; Sun, B. *J. Mater. Chem. C* **2015**, *3*, 4402.
(20) Dabrowski, A. J.; Iwanczyk, J. S.; Barton, J. B.; Huth, G. C. *IEEE Trans. Nucl. Sci.* **1981**, *28*, 536.
(21) López-Cruz, E.; Ramos, O. *Solid State Commun.* **1988**, *65*, 167.
(22) Hahn, T.; Shmueli, U.; Wilson, A. J. C.; International Union of Crystallography. *International Tables for Crystallography*; D. Reidel Publishing Company: Dordrecht, The Netherlands, 1984.
(23) George, M. A.; Chen, K.-T.; Collins, W. E.; Burger, A.; Nason, D.; Boatner, L. *J. Vac. Sci. Technol. B* **1996**, *14*, 1096.
(24) Prevot, B.; Schwab, C.; Dorner, B. *Phys. Status Solidi B* **1978**, *88*, 327.
(25) Skachkov, S. I.; Tyuterev, V. G. *Phys. Solid State* **1998**, *40*, 537.
(26) Sim, H. K.; Chang, Y. C. *Phys. Rev. B* **1994**, *49*, 4559.
(27) Seals, R. D.; Alexander, R.; Taylor, L. T.; Dillard, G. J. *Inorg. Chem.* **1973**, *12*, 2485.
(28) Bao, X. J.; Schlesinger, T. E.; James, R. B.; Ortale, C.; van der Berg, L. *J. Appl. Phys.* **1990**, *68*, 2951.
(29) Merz, J. L.; Wu, Z. L.; van den Berg, L.; Schnepple, W. F. *Nucl. Instrum. Methods Phys. Res.* **1983**, *213*, 51.
(30) Bao, X. J.; Schlesinger, T. E.; James, R. B.; Harvey, S. J.; Cheng, A. Y.; Gerrish, V.; Ortale, C. *Nucl. Instrum. Methods Phys. Res., Sect. A* **1992**, *317*, 194.
(31) Wen, X. M.; Xu, P.; Ohno, N. *J. Phys. Chem. S.* **2002**, *63*, 2107.
(32) Gonzalez, M.; Ibarra, A. *Phys. Rev. B* **1995**, *51*, 13786.
(33) Ayresa, F.; Machadoa, W. V. M.; Justob, J. F.; Assali, L. V. C. *Physica B* **2003**, *340*−*342*, 918.
(34) Akopyan, I. K.; Bondarenko, B. V.; Volkova, O. N.; Novikov, B. V.; Pavlova, T. A. *Phys. Solid State* **1997**, *39*, 58.
(35) Varshni, Y. P. *Physica* **1967**, *34*, 149.
(36) López-cruz, E. *J. Appl. Phys.* **1989**, *65*, 874.
(37) Ahuja, R.; Eriksson, O.; Johansson, B. *Phys. Rev. B* **1996**, *54*, 10419.
(38) Burger, A.; Nason, D.; Franks, L. *J. Cryst. Growth* **2013**, *379*, 3.


DOI: 10.1021/acs.cgd.5b00468
*Cryst. Growth Des.* XXXX, XXX, XXX−XXX